

Location-Aware Self-Supervised Transformers for Semantic Segmentation

Mathilde Caron Neil Houlsby Cordelia Schmid
Google Research

Abstract

Pixel-level labels are particularly expensive to acquire. Hence, pretraining is a critical step to improve models on a task like semantic segmentation. However, prominent algorithms for pretraining neural networks use image-level objectives, e.g. image classification, image-text alignment à la CLIP, or self-supervised contrastive learning. These objectives do not model spatial information, which might be sub-optimal when finetuning on downstream tasks with spatial reasoning. In this work, we pretrain network with a *location-aware (LOCA)* self-supervised method which fosters the emergence of strong dense features. Specifically, we use both a patch-level clustering scheme to mine dense pseudo-labels and a relative location prediction task to encourage learning about object parts and their spatial arrangements. Our experiments show that LOCA pretraining leads to representations that transfer competitively to challenging and diverse semantic segmentation datasets.

1. Introduction

The spatial annotations required for training semantic segmentation models are extremely time consuming and costly to acquire. Therefore, pretraining is commonly used to improve performance and label-efficiency of these models [61]. The dominant method for pretraining neural networks uses image-level tasks on massive amounts of supervised data [14, 53, 56, 78, 81]. For example, powerful foundation models such as Flamingo [2], CoCa [77] or PaLI [16], build upon a visual encoder pretrained by matching aligned image and text pairs with a contrastive loss [53], or by classifying images into a predefined set of categories [81]. These two standard supervised pretraining objectives operate at the global (whole image) level, without explicitly encouraging spatial reasoning.

However, it is unclear whether image-level pretraining is the optimal strategy when targeting recognition tasks with spatial understanding such as semantic segmentation. In fact, a recent study by Minderer *et al.* [47] shows that some

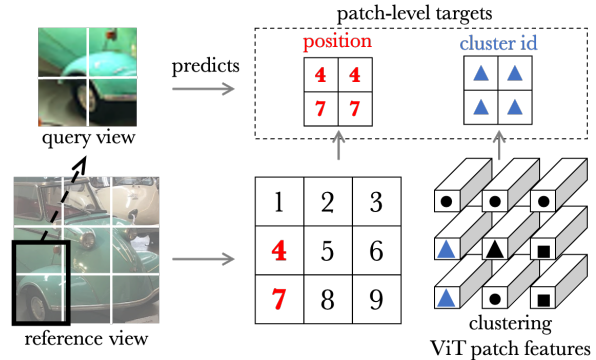


Figure 1. **LOCA** is a self-supervised pretraining method which combines relative position and patch-level cluster prediction. This achieves improved transfer on semantic segmentation datasets. The method is presented in Sec. 3.

models pretrained with image classification, while being excellent at image-level downstream tasks, transfer poorly to object detection, a task also requiring spatial reasoning. We argue that the main reason why pretraining is usually done with global objectives is because annotations are much easier to collect at the image level rather than at the pixel level. Indeed, the image classification or image-text datasets typically used in state-of-the-art systems [53, 81] are orders of magnitude bigger and cover more categories than densely annotated datasets [42, 83]. Therefore, one approach to unlock the potential of dense, spatially-aware pretraining at scale might be to move away from annotations, as proposed by self-supervised learning (SSL) approaches. A successful branch of SSL, often coined as “contrastive learning”, works by matching the representation of different views obtained from a same image by means of data augmentation [12, 15, 32, 35]. Interestingly, Caron *et al.* [13] have shown that segmentation masks emerge from the attention maps of Vision Transformers (ViT) [26] trained with these contrastive methods and several works have built on this observation to generate completely unsupervised segmentations [33, 58, 85]. However, we found in our preliminary experiments that salient attention maps do not correlate with superior performance after *finetuning* to the semantic segmentation task [85]. We hypothesize that this is because contrastive methods operate at the global level

Correspondence: mcaron@google.com. Code released at: <https://github.com/google-research/scenic/tree/main/scenic/projects/loca>

without explicitly encouraging spatial relationships. Worse, due to their intensive use of spatial data augmentation such as cropping and rescaling, they tend to produce *localization-invariant* features discarding spatial information [4, 18].

In order to foster the emergence of strong dense representations, our goal is to design a patch-level pretext task encouraging spatial localization reasoning. Recently, patch-level SSL pretrainings have attracted more and more attention in the community [5, 6, 34, 70, 74, 80]. For example, dense contrastive approaches adapt the popular contrastive SSL paradigm to the patch level [52, 55, 68, 72, 73] while masked autoencoders propose to reconstruct masked patches [6, 34]. Of particular interest, Zhai *et al.* [80] propose a pure localization method, that of predicting the patches position in an image. Intuitively, position prediction should inherently require a strong spatial and semantic understanding and has been the core motivation of the pioneering SSL branch of “jigsaw puzzle” [25, 50]. In this work, we propose to revisit this strategy and introduce a relative position prediction task. Specifically, our method works by predicting the location of a *query* view relatively to another, *reference*, view. To be able to locate themselves in the reference, the query patch features “look” at those of the reference through shallow cross-attention. We control the difficulty of the task and properties of the resulting features by masking reference patch features visible to the query. Our experiments show that this query-reference mechanism improves greatly over the single-view design of Zhai *et al.* [80] when transferring to semantic segmentation.

Since semantic segmentation is a per-patch classification problem, we also propose to prepare the ViT features for this task by means of clustering-based pseudo-labeling [3, 10, 75] done at the patch level [85]. Overall, we present in this work a **location-aware** (LOCA) self-supervised pretraining approach for semantic segmentation, which combines a straightforward patch-level SSL clustering method and relative position pretraining, as illustrated in Fig. 1. We show that LOCA yields improved performance over state-of-the-art supervised [53, 60, 65] and unsupervised [13, 17, 34, 84] representation learning methods for ViTs when transferred to 11 diverse and challenging semantic segmentation benchmarks. Our method scales promisingly to large models and large amount of data, which is a positive signal that it could be a viable candidate for spatially-aware pretraining at scale. Finally, we present a thorough analysis of different design choices which have led to the development of LOCA.

2. Related Work

Clustering-based SSL consists in using clustering while training to mine pseudo-labels in a dataset without annotations [10, 75]. This pseudo-assignment strategy is usually done at the image level [3, 4, 10, 12, 75] but recent works pro-

pose to cluster patch-level representations [19, 85]. In particular, our work takes inspiration from Leopart [85] which propose a patch-level cluster prediction task. However, unlike Leopart, our work leverages an explicit position-based pretraining and simplifies the clustering pipeline. For example, we omit foreground attention-based pooling, a design choice which makes Leopart a method that starts from an already good backbone [13] while ours trains from scratch.

SSL with location prediction. Pioneering works in SSL proposed to exploit spatial cues to generate pretext tasks [25, 31, 39, 41, 49, 50, 57]. Notably, inspired by word2vec [46], Doersch *et al.* [25] train a network to predict the relative position of a pair of patches from the same image while Noroozi and Favaro [50] extend this approach to solving “jigsaw puzzles” by rearranging a set of shuffled crops of an image. These approaches were developed with Convnets and very little work has revisited them in the scope of Transformers [80]. Zhai *et al.* [80] propose to pre-train a ViT to predict the position of its input patches given their visual appearance only, i.e. by discarding positional embeddings. We compare this strategy to the LOCA mechanism in Fig. 3 and Sec. 5.1. Also using localization, UP-DETR [22] propose to pretrain the DETR [9] architecture without using any annotations by localizing random boxes in a reference image. Our initial design is inspired by UP-DETR, though our implementations vary greatly: we formulate our task as a patch position classification problem while they follow DETR losses and architecture.

Context and masked auto-encoders. Also exploiting spatial cues for SSL, Pathak *et al.* [51] propose context auto-encoders to train Convnets to generate the content of a masked region based on its surrounding. Recently, masked auto-encoders revisit this “inpainting” approach to pretraining Vision Transformers [6, 34, 69]. Specifically, the task is to reconstruct masked [6] or dropped [34] patches from the input sequence tokens, either directly in pixel space [34] or in feature space [6, 69, 84]. Similar to our approach, masked auto-encoders are trained with patch-based objectives with a task encouraging the network to learn local representations of object parts and their spacial arrangement.

Dense contrastive SSL. A prominent line of SSL, often referred to as “contrastive” or “siamese” approaches, trains networks by matching the representation of different views obtained from a same image by means of data augmentation [4, 12, 15, 27, 32, 35, 71]. These approaches have primarily been developed with global (image-level) objectives but several recent works have adapted them to learn local features [37, 52, 55, 68, 72, 73, 79]. Specifically, instead of matching representations from global descriptors, they match features that come from the same location in the original image but seen from different views [52]. We borrow the strategy of back-tracking the data augmentation process of two views to find their regions that intersect [52].

Unsupervised semantic segmentation. While our goal is to improve pretraining for semantic segmentation, some parallel works to ours directly target semantic segmentation without using any supervision at all [19, 66]. Indeed, Caron *et al.* [13] have shown that unsupervised segmentation masks emerge from the attention module of ViTs trained with image-level contrastive objectives such as DINO. Several works build on this observation and enhance SSL features to produce completely unsupervised segmentations [33, 58, 85]. These approaches typically do not evaluate semantic segmentation after end-to-end finetuning.

3. Methodology

In order to foster the emergence of strong dense representations for semantic segmentation, we design LOCA, a patch-level SSL pretraining task that requires to reason about spatial localization. It works as a query-reference scheme where patches of a query view predict both their position and their cluster assignment relatively to a reference view, as illustrated in Fig 1.

Generating query and reference views. From an image x of a dataset, we form a *reference* view (denoted by x_{ref}) and a *query* view (denoted by x_q) using a randomized data augmentation routine composed of flipping, cropping, rescaling and color jittering. Because query and reference are generated by two independent augmentation draws, they usually have different image statistics (i.e. different scale, region or color histogram). This forces the network to rely less on low-level cues (chromatic aberration, color, and edge consistency) to solve the self-supervised task and more on recognizing object parts and their organization.

The query’s predictions are supervised by the reference view and therefore our loss is defined only at the intersection of the two views. Hence, we want the query and reference to intersect often. Also, we wish to constrain the spatial extent of the queries in order to favor the emergence of image-*part* representations. A natural choice then is to sample the reference view so that it covers a large area of the original image and the query views so that they cover a small portion of the original image. In practice we use the MSN input pipeline [4] with random resize-cropping and patch-dropping for generating different query views per reference. We consider a single query when describing the method for simplicity but use ten in our experiments.

Correspondences between query and reference. Following the standard protocol of the Vision Transformers [26], query and reference views are divided into non overlapping patches of resolution $P \times P$. More precisely, the reference view is flattened into $N_{ref} = \lfloor H_{ref}/P \rfloor \times \lfloor W_{ref}/P \rfloor$ (with $H_{ref} \times W_{ref}$ the resolution of x_{ref}) separate patches $\mathbf{x}_{ref}^i, i \in \{1, \dots, N_{ref}\}$. Default typical values are $H_{ref} = W_{ref} = 224, P = 16$ and $N_{ref} = 196$. A similar “patchification” process is applied on the query view,

resulting in a sequence of N_q patches $\mathbf{x}_q^j, j \in \{1, \dots, N_q\}$. Unless specified otherwise, we have $N_q = 36$. By backtracking the data augmentation draws that generated x_{ref} and x_q , we can identify the patch-level correspondences between these two views. In particular, we know a function \mathbf{h} that, given any patch position j in the query view, returns the position $i = \mathbf{h}(j)$ of the patch in the reference, $\mathbf{x}_{ref}^{\mathbf{h}(j)}$, that has the greatest overlap with the query patch \mathbf{x}_q^j . We implement the function \mathbf{h} with successive nearest interpolations and because the patchification grids of x_q and x_{ref} are usually not exactly aligned, a pair of matching patches, \mathbf{x}_q^j and $\mathbf{x}_{ref}^{\mathbf{h}(j)}$, have similar content but do not generally match *perfectly*. This effect can be seen in the example in Fig. 1.

Patch-level encoding with ViT. We process both the reference and query views with a Vision Transformer network [26], denoted by f , of internal dimension d ($d = 768$ for ViT-B). We note $\mathbf{Z}_q \in \mathbb{R}^{d \times N_q}$ (resp. $\mathbf{Z}_{ref} \in \mathbb{R}^{d \times N_{ref}}$), the output patch-level representation matrix of the query (resp. reference) view. As commonly done in SSL [12, 15, 32], we project these representations with a 2-layer multilayer perceptron (MLP), resulting in features $\tilde{\mathbf{Z}}_q \in \mathbb{R}^{\tilde{d} \times N_q}$ and $\tilde{\mathbf{Z}}_{ref} \in \mathbb{R}^{\tilde{d} \times N_{ref}}$ with $\tilde{d} = 256$.

Patch-level clustering. Training for semantic segmentation in a supervised setting is typically cast as a per-patch classification problem over K predefined categories:

$$\frac{1}{N_q} \sum_{j=1}^{N_q} \ell((Q^T \tilde{\mathbf{Z}}_q)_j, y_j)$$

where Q is a matrix in $\mathbb{R}^{\tilde{d} \times K}$ of learnable category prototypes and ℓ is the softmax cross-entropy loss. This problem is supervised by patch-level annotations y_j . However, because we do not have access to any annotations, inspired by previous SSL works [10, 12], we resort to clustering for pseudo-supervision. In particular, to supervise the patch j in the query, we cluster the patch representations of another view of the same image, i.e. the reference view. we obtain a soft cluster assignment (or pseudo-label) based on the similarity between the prototypes and the patch representation at the corresponding localization in the reference view:

$$\mathbf{y}_{ref}^i = \text{softmax}(\tilde{\mathbf{Z}}_{ref}^i \cdot Q / \tau)$$

with $i = \mathbf{h}(j)$ and τ a temperature parameter controlling the sharpness of the distribution. We further adjust the cluster assignment distribution with Sinkhorn-Knopp [21] to avoid the collapsing trivial solution [3, 12] and to encourage using equally all the clusters. Now that we have replaced expensive per-patch label supervision with cluster pseudo-labels we can minimize the following objective:

$$\frac{1}{|\Omega|} \sum_{j \in \Omega} \ell((Q^T \tilde{\mathbf{Z}}_q)_j, \mathbf{y}_{ref}^{\mathbf{h}(j)}) \quad (1)$$

Table 1. **Comparison with other SSL pretrainings on 11 semantic segmentation benchmarks.** We report mean IoU on the different validation sets. All methods use ImageNet-1k and ViT-B/16. We use the linear decoder from Segmenter [61] and run evaluation for other methods from their publicly released checkpoints. In the last column, we report the relative improvement over starting from random init. averaged across the 11 datasets. LOCA improves over MAE by +4.3 points.

Pretraining method	Consumer			Driving			Indoor	Aerial	Underwater	Avg. rel.		
	ADE20k	P.Cont	P.VOC	Citys.	BDD	CamVid	IDD	KITTI	SUN	ISPRS	SUIM	Δ (%)
Random init.	21.1	19.6	29.1	51.4	40.2	43.3	45.2	39.0	19.7	28.1	53.0	0
Supervised - DeiT-III [65]	47.3	53.9	76.1	79.7	62.7	53.8	55.4	47.2	47.5	42.1	73.5	79.0
DINO [13]	44.1	50.7	74.1	78.4	60.7	51.5	54.3	46.4	44.4	41.5	71.2	71.9
MoCo-v3 [17]	45.4	51.6	74.5	78.6	60.4	51.1	53.7	45.7	45.6	42.1	72.6	73.6
iBOT [84]	47.0	54.6	75.0	79.8	62.1	51.5	55.5	47.0	46.3	42.2	73.2	77.7
MAE [34]	45.5	51.7	75.0	79.7	62.1	57.8	55.8	48.3	45.9	44.6	72.4	77.8
LOCA (Ours)	47.9	54.9	76.7	79.8	62.8	56.1	55.6	48.5	47.7	45.6	74.0	82.1

where Ω is the set of patch position in the query that has an intersection with the reference (i.e. where \mathbf{h} is defined). We regularize this loss function with the mean entropy maximization (me-max) protocol [4] to encourage the network to use the full set of pseudo-label prototypes Q (see Tab. 6a)).

Patch position prediction. To encourage the network to learn about different object parts and their spatial arrangement, we propose to predict relative patch positions. We implement a query localization problem as a N_{ref} -way classification task where each query patch representations has to predict the position of the patch covering the same content in the reference view, as given by \mathbf{h} . To that end, the patch representations of the query need to be able to “look” at those of the reference. We implement this query-reference interaction with a single cross-attention transformer block, denoted by g , whose queries are computed from \mathbf{Z}_q and keys and values are obtained from \mathbf{Z}_{ref} . We denote the query representations after they have looked at the reference as $\mathbf{G} = g(\mathbf{Z}_q, \mathbf{Z}_{ref}) \in \mathbb{R}^{d \times N_q}$ and by $W \in \mathbb{R}^{d \times N_{ref}}$ the final “position classification” layer. Note that N_{ref} is the total number of positions in the reference. We train the network to minimize the following position prediction loss:

$$\frac{1}{|\Omega|} \sum_{j \in \Omega} \ell((W^T \mathbf{G})_j, \mathbf{h}(j)) \quad (2)$$

where Ω and ℓ are defined as in Eq 1.

Masking reference patch features visible to the query.

In practice, we find that problem 2 can be solved near perfectly by the network (see the validation accuracy in Fig. 4). As empirically shown in Sec. 5.1, one strategy to make the task more challenging is to restrict what the query can see from the reference. We implement this mechanism by randomly dropping (or “masking”) a ratio η of the patch features input to the cross-attention block g . Specifically, we redefine $\mathbf{G} = g(\mathbf{Z}_q, m(\mathbf{Z}_{ref}, \eta))$ where m is a random process that discards $\lfloor \eta N_{ref} \rfloor$ columns of \mathbf{Z}_{ref} . We use structured dropping (i.e. we keep a consecutive subset of patch

tokens) as we find in our experiments that it leads to superior performance than unstructured dropping (+0.8 mIoU).

Optimization. We train LOCA by minimizing the sum of the objectives in Eq 1 and Eq 2, averaged both over the different query views and the minibatch. We learn the parameters of f , g , Q , and W by back-propagating in the branch processing the query views. The parameters used in the branch processing the reference views are updated via an exponential moving average of the encoder parameters processing the query views [13, 32, 35]. This asymmetry improves performance and stability for clusters prediction and does not have any effect on the position prediction.

Implementation and evaluation. We train LOCA with learning rate of 0.001 (cosine schedule), batch size of 1024 and weight decay of 0.1 with adamw [43]. Models in Sec. 4 are trained for 600 epochs and those for analyses (Sec. 5) for 100 epochs. We evaluate by end-to-end finetuning on 11 semantic segmentation benchmarks [45]: ADE20k [83], Pascal Context (“P.Cont”) [48], Pascal VOC (“P.VOC”) [28], Cityscapes (“Citys.”) [20], Berkeley Deep Drive (“BDD”) [76], CamVid [8], India Driving Dataset (“IDD”) [67], KITTI [1], SUN-RGB-D (“SUN”) [59], ISPRS [44] and SUIM [38]. We follow and reproduce the linear decoder protocol of [61]. It uses a minimal amount of adapter layers to prevent the effect of pretraining of being washed out by heavy decoders. We report results for other methods if available and run evaluation from released checkpoints if not. We run a hyperparameter search with the same budget for all methods. We report results in single scale, averaged over 5 runs. All implementation details are in the Appendix A.

4. Main Results

4.1. Comparison with other SSL pretrainings

In this section, we compare LOCA to popular state-of-the-art SSL models for ViTs: DINO [13], MoCo-v3 [17], MAE [34] and iBOT [84]. The compared models all use ImageNet-1k (without labels) and ViT-B/16.

Table 2. **Fewshot semantic segmentation.** We report mean IoU on the validation set of ADE20k for different SSL pretrained models. All methods use ImageNet-1k and ViT-B/16. Only a fraction of training images are used for finetuning. Results are averaged over 5 different splits.

Method	1/32	1/16	1/8	1/4	1/2	1
Supervised - DeiT-III [65]	20.9	27.1	32.7	38.3	42.0	47.3
DINO [13]	18.4	24.5	29.5	35.2	39.5	44.1
MoCo-v3 [17]	17.7	25.2	30.8	36.5	40.7	45.4
iBOT [84]	20.9	28.0	33.4	38.7	42.6	47.0
MAE [34]	18.4	25.3	30.5	36.1	40.6	45.5
LOCA (Ours)	22.2	30.0	34.4	39.1	42.8	47.9

Transfer to 11 semantic segmentation benchmarks. In Tab. 1, we report the performance of different SSL pretraining strategies after end-to-end finetuning on semantic segmentation on diverse datasets. We observe that representations learned with LOCA transfer very well to semantic segmentation. Of particular interest, MAE representations achieve the second best SSL performance. In terms of training efficiency, based on our implementation, one LOCA epoch takes 17.4 minutes while one MAE epoch takes 5.7 minutes. However, LOCA reaches 82.1% average relative improvement over random initialization in 600 epochs while MAE reaches 77.8% in $2.6\times$ more epochs (1600). Hence, LOCA achieves an improvement of +4.3 points over MAE while being only $1.1\times$ longer to pretrain.

Label-efficient semantic segmentation. A good property for pretrained representations is the ability to transfer with few annotations [2, 4, 82]. In Tab. 2 we evaluate features when finetuning on fewshot semantic segmentation. In particular, we follow [36] and randomly sample a fraction of training images from ADE20k and use only those to finetune our model. In the 1/32 split, as few as 630 training images are used. We report the average over 5 different folds [36]. We observe that our spatially-aware pretraining improves label-efficiency of semantic segmentation models. The gap with previous methods becomes larger when very few images are available for finetuning.

4.2. Comparison with other pretraining paradigms

In this section, we compare our self-supervised location-aware pretraining to two powerful image-level pretraining paradigms: (i) image classification (i.e. label supervision) as in [60, 81] and (ii) image-text alignment as in CLIP [53].

Localization and classification trade-off. Semantic segmentation is the coupling of classification and localization, where these two tasks can have different feature preferences. In Tab 3, we disentangle classification and localization performance for models pretrained with an image-level versus spatially-aware objective. We evaluate performance on classification only by finetuning with a multi-label classification loss. We evaluate localization only by reporting

Table 3. **Comparison with supervised pretrainings** by disentangling localization and classification on semantic segmentation. We report classification only (“Classif.”: mAP), localization only (“Loc”: mIoU) and full semantic segmentation (“Both”: mIoU) on ADE20k. LOCA yields excellent locality and good semantic understanding. It is behind supervised image-level pretraining on the pure semantic axis (classification) but better on segmentation (“Both”).

Method	Data	Sup.	Loc-aware?	Classif.	Loc.	Both
<i>ViT-Base/16</i>						
CLIP [53]	WIT	Text		58.3	66.4	45.9
AugReg [60]	Im21k	Labels		60.7	67.4	48.1
LOCA (Ours)	Im21k	\emptyset	✓	50.2	68.5	48.5
<i>ViT-Large/16</i>						
AugReg [60]	Im21k	Labels		60.3	68.0	50.7
LOCA (Ours)	Im21k	\emptyset	✓	51.6	71.0	52.3

the performance when replacing the label of each mask by the label of the ground truth mask the model has the best IoU with. This allows to assess the shape and localization of the predictions but not their class. We report results for ADE20k in Tab. 3 and for other datasets in Table 7 in Appendix B.2. We observe that models pretrained with a global, image-level supervised objective are better than LOCA at classification. However, LOCA performs better at localization which results in improved performance on semantic segmentation which requires both locality and class-level understanding.

Depth estimation. The previous experiment (Tab. 3) shows that LOCA features are particularly good at localization. While the focus of this work is semantic segmentation, we explore the potential of LOCA on depth estimation, another per-pixel prediction task requiring high spatial understanding but less semantics than semantic segmentation. We follow [23] and train a Dense Prediction Transformer [54] with frozen backbone on the Waymo Open real-world driving dataset [62]. We observe in Tab. 4 that LOCA transfers better to depth estimation than backbones trained with image-level supervision. Notably, LOCA achieves comparable or better performance than supervised ViT-e while using more than $10\times$ less parameters.

4.3. Scaling data and model axes

A premise of SSL is that it can scale to arbitrary large datasets since images don’t require any annotations. Because location-aware *supervised* pretraining is not feasible in practice due to the huge cost of pixel-level annotations, we believe our self-supervised spatial pretraining could be a good candidate for scaling. In Fig 2, we propose a scaling study on data (left panel) and model (right panel) axes. We observe that LOCA Large architecture benefits more from scaling in dataset size than the smaller Base architecture. Also, we see that pretraining LOCA on the full ImageNet-

Table 4. **Monocular depth estimation** on the Waymo Open dataset [62]. We follow the setup from [23] and report their number for ViT-L and ViT-e supervised (“sup”) backbones.

Model	param(M)	MSE ↓	AbsRel ↓	$\delta \uparrow$		
				< 1.1	< 1.25	< 1.25 ²
ViT-L sup [60]	304	0.027	0.121	0.594	0.871	0.972
ViT-L LOCA	304	0.024	0.102	0.681	0.891	0.973
ViT-e sup [81]	3926	0.024	0.112	0.631	0.888	0.975
ViT-H LOCA	632	0.024	0.101	0.685	0.894	0.975

21k scales better in model axis than using the smaller, albeit highly curated, ImageNet-1k dataset. This is not the case for some previous self-supervised learning methods as recently observed by [40]. Overall, mirroring the trend of image-level supervised pretrainings [16, 81], we observe that we need to scale both dataset size and model capacity to achieve the best of performance. While these preliminary results give promising signal about LOCA scalability, we note that ImageNet-21k is a relatively curated dataset and we would still need to probe our model on large, *uncurated* data [11, 30, 40, 63].

5. Design Choices Analyses

In this section, we detail various design choices for LOCA. First, we make an in-depth study of the position prediction. Second, we present an ablation study focused on the pseudo-labeling clustering technique.

5.1. Position prediction framework

To encourage the network to learn about the spatial arrangement of different object parts, we propose to predict relative positions. We detail here different components of our framework: the query-reference mechanism, the effect of masking reference patches and the loss function. Unless specified otherwise, models are trained solely with loss (2) in this section to isolate the effect of position-based training.

Query-reference. We compare the two mechanisms illustrated in Fig. 3. The “single” strategy is akin to Zhai *et al.* [80]. Because position prediction is trivial in single view with positional embeddings [80], we remove them in this experiment to avoid confounding factors. We vary η the proportion of masked patch tokens. In “single”, masking patch tokens means that patches can only attend to the unmasked ones, i.e. only the unmasked patches take part in the computation of attention keys and values [80]. Results are in Fig. 4. On the left, we report the validation accuracy for the position prediction task. This measures how well the network solves its pretraining objective in a fixed training budget, which enables the comparison of the difficulty of different pretraining strategies. On the right, we show transfer performance.

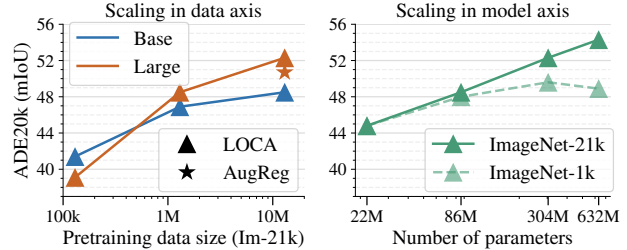


Figure 2. **Scaling study.** We report transfer on ADE20k validation set. Scaling both dataset size and model capacity results in the best of transfer performance.

We see in Fig. 4 that the query-reference mechanism of LOCA is a more challenging pretraining framework than Zhai *et al.* [80] and leads to better representations for semantic segmentation (+7.6 mIoU). This can intuitively be explained by several conceptual differences. First, in [80], the network can almost perfectly solve the task by leveraging low-level non-semantic cues such as chromatic aberration, color or edges consistency between patches. This is *partly* prevented in the query-reference mechanism due to different image statistics between query and reference (thanks to cropping, rescaling and color jittering). Second, the way query (i.e. patches that predict a position) and reference (i.e. context patches) can interact is in stark contrast in the two mechanisms. In “single”, query and reference interact in an unconstrained manner at all stages of the computation. With masking, this design is partly modified by processing each query patch independently but still allowing them to fully attend to the reference patches at each block. By contrast, in LOCA, query patches can attend freely to each other but cannot look at the reference patches until the last stage of the network. Intuitively, this more constrained interaction encourages both query and reference patches to develop stronger final localization features.

Masking reference patches. In Fig. 4, we observe that the localization pretraining task can be solved near perfectly when all the patches in the reference are visible to the query (see Fig. 4 left for $\eta = 0$). Masking to the query makes the pretraining objective more challenging and leads to better representations. In Fig. 5, we analyze this effect further. We consider different masking ratios and report for the same downstream dataset both the transfer performance on semantic segmentation and multi-label classification (with frozen backbone) by turning the semantic segmentation annotations into classification labels. We observe in Fig. 5 that masking improves both localization and classification capabilities of the network. Intuitively this is because masking reference patches forces the query to rely less on finding matching salient points between the two views and more on recognizing objects and their parts as illustrated in Fig 6.

However, when masking is too aggressive, the query does not see enough of the reference to solve its task by

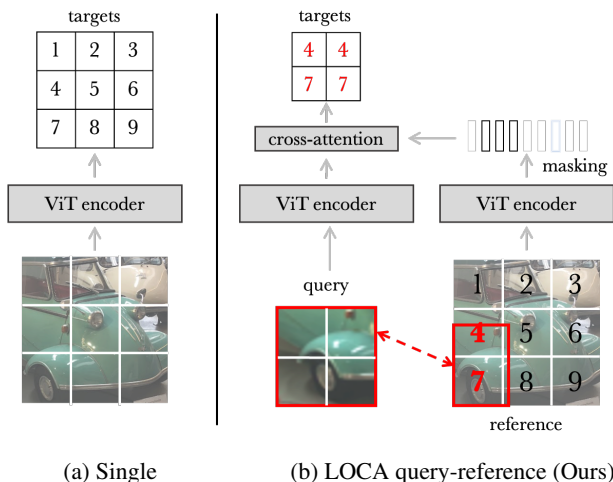


Figure 3. **Conceptual comparison of single vs query-reference** patch position prediction mechanisms: (a) in a single view as in Zhai *et al.* [80]; (b) in a query view relatively to a reference view as in LOCA (Ours). Quantitative comparison is in Fig. 4. Masking not illustrated for single.

relative localization and resorts to other cues. To understand this phenomenon, we push masking to extreme rates and even report performance when the reference is *not visible at all* ($\eta = 1$). Surprisingly, we find that the query still manages to solve the localization pretraining task to some extent with a localization accuracy of 3.7% (random guessing achieves 0.5%). We hypothesize that two ways of solving the task without looking at the reference are to (i) learn where things are typically located in images and (ii) memorize all the dataset images. We argue that the “memorization” regime is akin to an implicit formulation of the “exemplar” instance discrimination approach of Dosovitskiy *et al.* [27] where the network learns to recognize each individual instance of a dataset (but without a classifier of the size of the dataset as in [27]). Overall, both learning biases of general dataset statistics and instance discrimination have been shown to improve transfer performance on classification downstream tasks [27, 29, 71] which is consistent with the boost in classification observed for $\eta = 1$.

Finally, this experiment shows that an optimal masking ratio for semantic segmentation features is high, but not too high either so that the network can still solve the task by *relative localization*. In practice, we use $\eta = 0.8$.

Choice of localization loss. First, we compare predicting the position of all patches versus the position of the central patch only. We see in Tab. 5 that all patches is better. We hypothesize that this is because it requires to predict the spatial extent of the query and not just an anchor point. Second, we compare solving a per-patch position classification problem versus regressing the coordinates of the query box in the reference. For box prediction, we use a linear combination of ℓ_1 loss and the generalized IoU loss, following UP-DETR [9, 22]. Because query and reference patchifica-

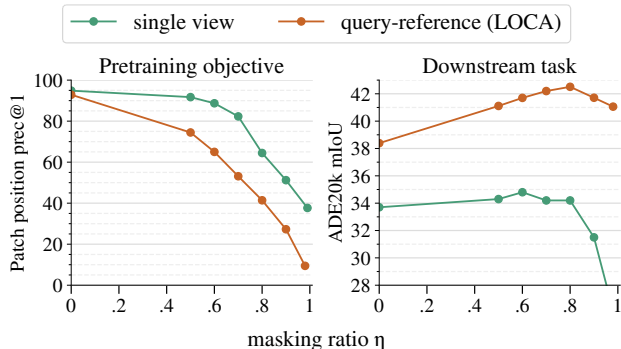


Figure 4. **Single vs query-reference** patch position prediction mechanisms. For both mechanisms, we report the position prediction accuracy (left) and the performance after transfer to semantic segmentation on ADE20k (right) for different patch masking ratios η . Query-reference makes for a more challenging pre-training objective (lower accuracy on the position prediction task) due to different image statistics between query and reference and constrained patch interactions. Conceptual differences are illustrated in Fig. 3. Varying the masking ratio controls the difficulty of the task and improves transfer performance.

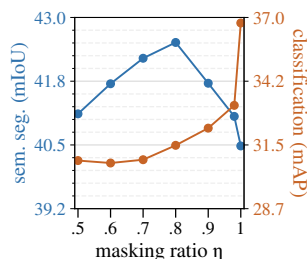


Figure 5. **Masking reference patches to the query** improves both classification and segmentation on ADE20k. Too much masking prevents the query from solving the task by spatial reasoning which hurts segmentation.

tion grids are usually not aligned, matching patches in query and reference do not have exactly the same content. This does not affect the box regression formulation, which might give it an advantage over per-patch classification. However, we surprisingly find in Tab. 5 that box regression leads to poorer performance than per-patch classification. It is possible that this loss requires additional hyper-parameter tuning (we use the default in [9, 22]). Overall, position classification is a simple implementation of the relative localization problem and works well in practice.

Combining with patch clustering. In the previous experiments, we have validated our position prediction scheme and showed that it improves by +7.6mIoU over the position prediction method of Zhai *et al.* [80]. While we find that predicting position only is performing less well than predicting patch-level cluster assignments only (−3.3mIoU) the best performance is obtained when predicting *both* (+0.7mIoU over cluster only) which demonstrates some complementary between them.

Visualizing LOCA’s predictions. In Fig. 6, we visualize the output of location prediction models trained with different masking rates: $\eta = 0$ (no masking), $\eta = 0.8$ (default) and $\eta = 1$ (invisible reference). The first row shows a sit-

Table 5. **Localization loss.** We report mIoU on ADE20k for different loss variants. Predicting the position of all patches *vs* the position of the central patch only is better, likely because it involves reasoning about the spatial extent of the query. Classification works better than regression in our experiment, despite the fact that regression is not impacted by the misalignment between query and reference patch grids.

Output	Predicts spatial extent	Loss	ADE20k
Every patch position	✓	Classif.	42.5
Central patch position		Classif.	38.6
Query box coordinates	✓	Regress.	39.0

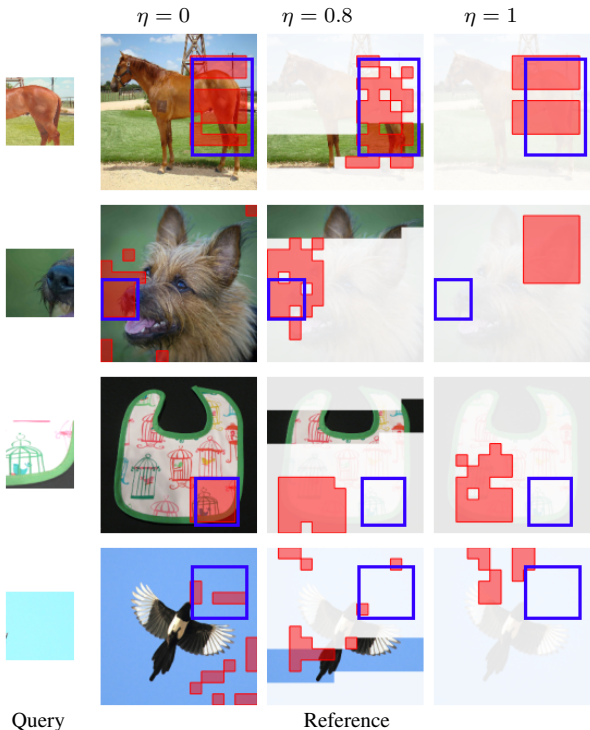


Figure 6. **Visualizing LOCA’s predictions.** The query location is shown in blue in the reference and LOCA predictions are shown in red. Columns correspond to different reference masking rates and we show only patches visible to the query. More examples in the Appendix C. Displayed images are not seen during training.

uation where the network can make a valid guess about the query’s location solely based on the query visual appearance, i.e. without looking at the reference. In the second row, we see that LOCA successfully locates the snout of the dog based on the reference ear patches. This suggests that it has learned about spatial arrangement of different parts of a dog. Third row depicts the case where the network can leverage low-level cues such as edge consistency to locate the query. The masked variants are restrained in their use of such cues and hence fail to locate the query. Finally, in last row, there is no visible cue in the query that allows its localization. The prediction is degenerated for all the variants.

a) SK and me-max encourage use of all prototypes. H: average prediction entropy.

SK	me-max	H	ADE20k
✓	✓	8.28	46.2
		8.27	46.1
	✓	8.14	45.7
		0	collapse

b) Patch-level clustering is better for transfer on semantic segmentation.

Cluster	classif. semseg.	
	Im1k-10s	ADE20k
Patch	40.9	46.2
Image (CLS)	48.6	43.8
Image (GAP)	48.5	43.8

c) Effect of the number of cluster prototypes.

K	2^4	2^8	2^{12}	2^{14}
ADE20k	45.3	46.2	46.2	45.8

d) Number of queries.

# queries	10	5	2	1
ADE20k	46.2	45.5	43.4	41.1
Speedup	-	$\times 1.5$	$\times 2.1$	$\times 3.0$

Table 6. **Ablation study of different design choices.**

5.2. Ablation study of patch clustering

In Tab. 6, we report model ablation results. In Tab. 6 a), we observe that both Sinkhorn-Knopp and me-max regularizations are useful to encourage the model to use the full set of cluster prototypes. In Tab. 6 b), we compare our patch-level pseudo-labeling method to image-level ones on ADE20k semantic segmentation and on ImageNet-1k 10-shot classification. The image-level clustering framework is akin to existing SSL frameworks such as DINO [13] or MSN [4]. We evaluate two global aggregation techniques: token (“CLS”) and global average pooling (GAP). We observe that performance on semantic segmentation is improved when considering per-patch assignments instead of image-level clustering. However, we observe a decay on classification. In Tab. 6 c), we see that the method is robust to the number of clusters K , though over-clustering is beneficial [10, 85]. In Tab. 6 d), we show the effect of reducing the number of queries. Using a single query instead of 10 allows to speed up pretraining time by $\times 3$ but induces a loss of 5.1mIoU in transfer performance.

6. Conclusion

We propose a SSL spatially-aware pretraining that transfers well to semantic segmentation. A promising direction for future work is to combine dense objectives with global image-level ones [7, 84]. Finally, we focus on semantic segmentation in this paper as it is representative of tasks requiring spatial reasoning. However, the set of visual task with localization is large and we hope that our findings can serve as a useful checkpoint for future studies beyond the scopes of semantic segmentation or even still images.

Acknowledgement. We thank Anurag Arnab, Lucas Beyer, Mostafa Dehghani, Ahmet Iscen, Thomas Kipf, Thomas Lucas, Thomas Mensink, Matthias Minderer, Basil

Mustafa as well as the entire Ganesha team and Grand Vision group for their precious help, support and discussions.

References

- [1] Hassan Abu Alhaija, Siva Karthik Mustikovela, Lars Mescheder, Andreas Geiger, and Carsten Rother. Augmented reality meets computer vision: Efficient data generation for urban driving scenes. *International Journal of Computer Vision*, 2018. [4](#), [12](#)
- [2] Jean-Baptiste Alayrac, Jeff Donahue, Pauline Luc, Antoine Miech, Iain Barr, Yana Hasson, Karel Lenc, Arthur Mensch, Katie Millican, Malcolm Reynolds, et al. Flamingo: a visual language model for few-shot learning. *arXiv preprint arXiv:2204.14198*, 2022. [1](#), [5](#)
- [3] Yuki Markus Asano, Christian Rupprecht, and Andrea Vedaldi. Self-labelling via simultaneous clustering and representation learning. In *ICLR*, 2020. [2](#), [3](#)
- [4] Mahmoud Assran, Mathilde Caron, Ishan Misra, Piotr Bojanowski, Florian Bordes, Pascal Vincent, Armand Joulin, Mike Rabbat, and Nicolas Ballas. Masked siamese networks for label-efficient learning. In *ECCV*, 2022. [2](#), [3](#), [4](#), [5](#), [8](#), [12](#)
- [5] Alexei Baevski, Wei-Ning Hsu, Qiantong Xu, Arun Babu, Jiatuo Gu, and Michael Auli. Data2vec: A general framework for self-supervised learning in speech, vision and language. *arXiv preprint arXiv:2202.03555*, 2022. [2](#)
- [6] Hangbo Bao, Li Dong, and Furu Wei. Beit: Bert pre-training of image transformers. *arXiv preprint arXiv:2106.08254*, 2021. [2](#)
- [7] Adrien Bardes, Jean Ponce, and Yann LeCun. Vicregl: Self-supervised learning of local visual features. In *NeurIPS*, 2021. [8](#)
- [8] Gabriel J. Brostow, Julien Fauqueur, and Roberto Cipolla. Semantic object classes in video: A high-definition ground truth database. *Patt. Rec. Letters*, 2009. [4](#), [12](#)
- [9] Nicolas Carion, Francisco Massa, Gabriel Synnaeve, Nicolas Usunier, Alexander Kirillov, and Sergey Zagoruyko. End-to-end object detection with transformers. In *ECCV*, 2020. [2](#), [7](#)
- [10] Mathilde Caron, Piotr Bojanowski, Armand Joulin, and Matthijs Douze. Deep clustering for unsupervised learning of visual features. In *ECCV*, 2018. [2](#), [3](#), [8](#)
- [11] Mathilde Caron, Piotr Bojanowski, Julien Mairal, and Armand Joulin. Unsupervised pre-training of image features on non-curated data. In *ICCV*, 2019. [6](#)
- [12] Mathilde Caron, Ishan Misra, Julien Mairal, Priya Goyal, Piotr Bojanowski, and Armand Joulin. Unsupervised learning of visual features by contrasting cluster assignments. In *NeurIPS*, 2020. [1](#), [2](#), [3](#)
- [13] Mathilde Caron, Hugo Touvron, Ishan Misra, Hervé Jégou, Julien Mairal, Piotr Bojanowski, and Armand Joulin. Emerging properties in self-supervised vision transformers. In *ICCV*, 2021. [1](#), [2](#), [3](#), [4](#), [5](#), [8](#), [12](#), [13](#), [14](#)
- [14] Joao Carreira and Andrew Zisserman. Quo vadis, action recognition? a new model and the kinetics dataset. In *CVPR*, pages 6299–6308, 2017. [1](#)
- [15] Ting Chen, Simon Kornblith, Mohammad Norouzi, and Geoffrey Hinton. A simple framework for contrastive learning of visual representations. *preprint arXiv:2002.05709*, 2020. [1](#), [2](#), [3](#)
- [16] Xi Chen, Xiao Wang, Soravit Changpinyo, AJ Piergiovanni, Piotr Padlewski, Daniel Salz, Sebastian Goodman, Adam Grycner, Basil Mustafa, Lucas Beyer, et al. Pali: A jointly-scaled multilingual language-image model. *arXiv preprint arXiv:2209.06794*, 2022. [1](#), [6](#)
- [17] Xinlei Chen, Saining Xie, and Kaiming He. An empirical study of training self-supervised vision transformers. In *ICCV*, 2021. [2](#), [4](#), [5](#), [13](#), [14](#)
- [18] Yubei Chen, Adrien Bardes, Zengyi Li, and Yann LeCun. Intra-instance vicreg: Bag of self-supervised image patch embedding. *arXiv preprint arXiv:2206.08954*, 2022. [2](#)
- [19] Jang Hyun Cho, Utkarsh Mall, Kavita Bala, and Bharath Hariharan. Picie: Unsupervised semantic segmentation using invariance and equivariance in clustering. In *CVPR*, 2021. [2](#), [3](#)
- [20] Marius Cordts, Mohamed Omran, Sebastian Ramos, Timo Rehfeld, Markus Enzweiler, Rodrigo Benenson, Uwe Franke, Stefan Roth, and Bernt Schiele. The cityscapes dataset for semantic urban scene understanding. In *CVPR*, 2016. [4](#), [12](#), [14](#)
- [21] Marco Cuturi. Sinkhorn distances: Lightspeed computation of optimal transport. In *NeurIPS*, 2013. [3](#)
- [22] Zhigang Dai, Bolun Cai, Yugeng Lin, and Junying Chen. Up-detr: Unsupervised pre-training for object detection with transformers. In *CVPR*, 2021. [2](#), [7](#)
- [23] Mostafa Dehghani, Josip Djolonga, Basil Mustafa, Piotr Padlewski, Jonathan Heek, Justin Gilmer, Andreas Steiner, Mathilde Caron, Robert Geirhos, Ibrahim Alabdulmohsin, et al. Scaling vision transformers to 22 billion parameters. *arXiv preprint arXiv:2302.05442*, 2023. [5](#), [6](#)
- [24] Mostafa Dehghani, Alexey Gritsenko, Anurag Arnab, Matthias Minderer, and Yi Tay. Scenic: A jax library for computer vision research and beyond. In *CVPR*, 2022. [12](#)
- [25] Carl Doersch, Abhinav Gupta, and Alexei A Efros. Unsupervised visual representation learning by context prediction. In *ICCV*, 2015. [2](#)
- [26] Alexey Dosovitskiy, Lucas Beyer, Alexander Kolesnikov, Dirk Weissenborn, Xiaohua Zhai, Thomas Unterthiner, Mostafa Dehghani, Matthias Minderer, Georg Heigold, Sylvain Gelly, et al. An image is worth 16x16 words: Transformers for image recognition at scale. *preprint arXiv:2010.11929*, 2020. [1](#), [3](#)
- [27] Alexey Dosovitskiy, Philipp Fischer, Jost Tobias Springenberg, Martin Riedmiller, and Thomas Brox. Discriminative unsupervised feature learning with exemplar convolutional neural networks. *TPAMI*, 2016. [2](#), [7](#)
- [28] Mark Everingham, Luc Van Gool, Christopher KI Williams, John Winn, and Andrew Zisserman. The pascal visual object classes (voc) challenge. *IJCV*, 2010. [4](#), [12](#), [14](#)
- [29] Spyros Gidaris, Praveer Singh, and Nikos Komodakis. Unsupervised representation learning by predicting image rotations. *arXiv preprint arXiv:1803.07728*, 2018. [7](#)

- [30] Priya Goyal, Mathilde Caron, Benjamin Lefaudeaux, Min Xu, Pengchao Wang, Vivek Pai, Mannat Singh, Vitaliy Liptchinsky, Ishan Misra, Armand Joulin, and Piotr Bojanowski. Self-supervised pretraining of visual features in the wild. *arXiv preprint arXiv:2103.01988*, 2021. 6
- [31] Priya Goyal, Dhruv Mahajan, Abhinav Gupta, and Ishan Misra. Scaling and benchmarking self-supervised visual representation learning. In *ICCV*, 2019. 2
- [32] Jean-Bastien Grill, Florian Strub, Florent Altché, Corentin Tallec, Pierre H Richemond, Elena Buchatskaya, Carl Doersch, Bernardo Avila Pires, Zhaohan Daniel Guo, Mohammad Gheshlaghi Azar, Bilal Piot, Koray Kavukcuoglu, Rémi Munos, and Michal Valko. Bootstrap your own latent: A new approach to self-supervised learning. In *NeurIPS*, 2020. 1, 2, 3, 4, 12
- [33] Mark Hamilton, Zhoutong Zhang, Bharath Hariharan, Noah Snavely, and William T Freeman. Unsupervised semantic segmentation by distilling feature correspondences. In *ICLR*, 2022. 1, 3
- [34] Kaiming He, Xinlei Chen, Saining Xie, Yanghao Li, Piotr Dollár, and Ross Girshick. Masked autoencoders are scalable vision learners. In *CVPR*, 2022. 2, 4, 5, 13, 14
- [35] Kaiming He, Haoqi Fan, Yuxin Wu, Saining Xie, and Ross Girshick. Momentum contrast for unsupervised visual representation learning. In *CVPR*, 2020. 1, 2, 4
- [36] Hanzhe Hu, Fangyun Wei, Han Hu, Qiwei Ye, Jinshi Cui, and Liwei Wang. Semi-supervised semantic segmentation via adaptive equalization learning. *NeurIPS*, 2021. 5
- [37] Lang Huang, Shan You, Mingkai Zheng, Fei Wang, Chen Qian, and Toshihiko Yamasaki. Learning where to learn in cross-view self-supervised learning. In *CVPR*, 2022. 2
- [38] Md Jahidul Islam, Chelsey Edge, Yuyang Xiao, Peigen Luo, Muntaqim Mehtaz, Christopher Morse, Sadman Sakib Enan, and Junaed Sattar. Semantic segmentation of underwater imagery: Dataset and benchmark. In *2020 IEEE/RSJ International Conference on Intelligent Robots and Systems (IROS)*, 2020. 4, 12
- [39] Dahun Kim, Donghyeon Cho, Donggeun Yoo, and In So Kweon. Learning image representations by completing damaged jigsaw puzzles. In *WACV*, 2018. 2
- [40] Skanda Koppula, Yazhe Li, Evan Shelhamer, Andrew Jaegle, Nikhil Parthasarathy, Relja Arandjelovic, João Carreira, and Olivier Hénaff. Where should i spend my flops? efficiency evaluations of visual pre-training methods. *arXiv preprint arXiv:2209.15589*, 2022. 6
- [41] Hsin-Ying Lee, Jia-Bin Huang, Maneesh Singh, and Ming-Hsuan Yang. Unsupervised representation learning by sorting sequences. In *ICCV*, 2017. 2
- [42] Tsung-Yi Lin, Michael Maire, Serge Belongie, James Hays, Pietro Perona, Deva Ramanan, Piotr Dollár, and C Lawrence Zitnick. Microsoft coco: Common objects in context. In *ECCV*, 2014. 1
- [43] Ilya Loshchilov and Frank Hutter. Fixing weight decay regularization in adam. 2018. 4, 12
- [44] Jochen Meidow, Melanie Pohl, Peter Solbrig, and Peter Wernerus. Theme section “urban object detection and 3d building reconstruction”. *ISPRS journal of photogrammetry and remote sensing*, 2014. 4, 12
- [45] Thomas Mensink, Jasper Uijlings, Alina Kuznetsova, Michael Gygli, and Vittorio Ferrari. Factors of influence for transfer learning across diverse appearance domains and task types. *IEEE TPAMI*, 2021. 4, 12
- [46] Tomas Mikolov, Kai Chen, Greg Corrado, and Jeffrey Dean. Efficient estimation of word representations in vector space. *arXiv preprint arXiv:1301.3781*, 2013. 2
- [47] Matthias Minderer, Alexey Gritsenko, Austin Stone, Maxim Neumann, Dirk Weissenborn, Alexey Dosovitskiy, Aravindh Mahendran, Anurag Arnab, Mostafa Dehghani, Zhuoran Shen, et al. Simple open-vocabulary object detection with vision transformers. *arXiv preprint arXiv:2205.06230*, 2022. 1
- [48] Roozbeh Mottaghi, Xianjie Chen, Xiaobai Liu, Nam-Gyu Cho, Seong-Whan Lee, Sanja Fidler, Raquel Urtasun, and Alan Yuille. The role of context for object detection and semantic segmentation in the wild. In *CVPR*, 2014. 4, 12, 14
- [49] T Nathan Mundhenk, Daniel Ho, and Barry Y Chen. Improvements to context based self-supervised learning. In *CVPR*, 2018. 2
- [50] Mehdi Noroozi and Paolo Favaro. Unsupervised learning of visual representations by solving jigsaw puzzles. In *ECCV*, 2016. 2
- [51] Deepak Pathak, Philipp Krahenbuhl, Jeff Donahue, Trevor Darrell, and Alexei A Efros. Context encoders: Feature learning by inpainting. In *CVPR*, 2016. 2
- [52] Pedro O Pinheiro, Amjad Almahairi, Ryan Y Benmaleck, Florian Golemo, and Aaron Courville. Unsupervised learning of dense visual representations. 2020. 2
- [53] Alec Radford, Jong Wook Kim, Chris Hallacy, Aditya Ramesh, Gabriel Goh, Sandhini Agarwal, Girish Sastry, Amanda Askell, Pamela Mishkin, Jack Clark, et al. Learning transferable visual models from natural language supervision. 2021. 1, 2, 5, 12, 13
- [54] René Ranftl, Alexey Bochkovskiy, and Vladlen Koltun. Vision transformers for dense prediction. In *ICCV*, 2021. 5
- [55] Byungseok Roh, Wuhyun Shin, Ildoo Kim, and Sungwoong Kim. Spatially consistent representation learning. In *CVPR*, 2021. 2
- [56] Olga Russakovsky, Jia Deng, Hao Su, Jonathan Krause, Sanjeev Satheesh, Sean Ma, Zhiheng Huang, Andrej Karpathy, Aditya Khosla, Michael Bernstein, Alexander C Berg, and Li Fei-Fei. Imagenet large scale visual recognition challenge. *IJCV*, 2015. 1
- [57] Rodrigo Santa Cruz, Basura Fernando, Anoop Cherian, and Stephen Gould. Deeppermnet: Visual permutation learning. In *CVPR*, 2017. 2
- [58] Oriane Siméoni, Gilles Puy, Huy V Vo, Simon Roburin, Spyros Gidaris, Andrei Bursuc, Patrick Pérez, Renaud Marlet, and Jean Ponce. Localizing objects with self-supervised transformers and no labels. *arXiv preprint arXiv:2109.14279*, 2021. 1, 3
- [59] Shuran Song, Samuel P Lichtenberg, and Jianxiong Xiao. Sun rgb-d: A rgb-d scene understanding benchmark suite. In *CVPR*, 2015. 4, 12
- [60] Andreas Steiner, Alexander Kolesnikov, Xiaohua Zhai, Ross Wightman, Jakob Uszkoreit, and Lucas Bayer. How to train

- your vit? data, augmentation, and regularization in vision transformers. *arXiv preprint arXiv:2106.10270*, 2021. 2, 5, 6, 12, 13
- [61] Robin Strudel, Ricardo Garcia, Ivan Laptev, and Cordelia Schmid. Segmenter: Transformer for semantic segmentation. In *ICCV*, 2021. 1, 4, 12, 13
- [62] Pei Sun, Henrik Kretzschmar, Xerxes Dotiwalla, Aurelien Chouard, Vijaysai Patnaik, Paul Tsui, James Guo, Yin Zhou, Yuning Chai, Benjamin Caine, et al. Scalability in perception for autonomous driving: Waymo open dataset. In *CVPR*, 2020. 5, 6
- [63] Yonglong Tian, Olivier J Henaff, and Aäron van den Oord. Divide and contrast: Self-supervised learning from uncurated data. In *ICCV*, 2021. 6
- [64] Hugo Touvron, Matthieu Cord, Matthijs Douze, Francisco Massa, Alexandre Sablayrolles, and Hervé Jégou. Training data-efficient image transformers & distillation through attention. *preprint arXiv:2012.12877*, 2020. 13
- [65] Hugo Touvron, Matthieu Cord, and Hervé Jégou. Deit iii: Revenge of the vit. *arXiv preprint arXiv:2204.07118*, 2022. 2, 4, 5, 13, 14
- [66] Wouter Van Gansbeke, Simon Vandenhende, Stamatios Georgoulis, and Luc Van Gool. Unsupervised semantic segmentation by contrasting object mask proposals. In *ICCV*, 2021. 3
- [67] Girish Varma, Anbumani Subramanian, Anoop Namboodiri, Manmohan Chandraker, and CV Jawahar. Idd: A dataset for exploring problems of autonomous navigation in unconstrained environments. In *WACV*, 2019. 4, 12
- [68] Xinlong Wang, Rufeng Zhang, Chunhua Shen, Tao Kong, and Lei Li. Dense contrastive learning for self-supervised visual pre-training. In *CVPR*, 2021. 2
- [69] Chen Wei, Haoqi Fan, Saining Xie, Chao-Yuan Wu, Alan Yuille, and Christoph Feichtenhofer. Masked feature prediction for self-supervised visual pre-training. In *CVPR*, 2022. 2
- [70] Philippe Weinzaepfel, Vincent Leroy, Thomas Lucas, Romain Brégier, Johann Cabon, Vaibhav Arora, Leonid Antsfeld, Boris Chidlovskii, Gabriela Csurka, and Jérôme Revaud. Croco: Self-supervised pre-training for 3d vision tasks by cross-view completion. In *NeurIPS*, 2022. 2
- [71] Zhirong Wu, Yuanjun Xiong, Stella X Yu, and Dahua Lin. Unsupervised feature learning via non-parametric instance discrimination. In *CVPR*, 2018. 2, 7
- [72] Tete Xiao, Colorado J Reed, Xiaolong Wang, Kurt Keutzer, and Trevor Darrell. Region similarity representation learning. In *ICCV*, 2021. 2
- [73] Zhenda Xie, Yutong Lin, Zheng Zhang, Yue Cao, Stephen Lin, and Han Hu. Propagate yourself: Exploring pixel-level consistency for unsupervised visual representation learning. In *CVPR*, 2021. 2
- [74] Zhenda Xie, Zheng Zhang, Yue Cao, Yutong Lin, Jianmin Bao, Zhuliang Yao, Qi Dai, and Han Hu. Simmim: A simple framework for masked image modeling. In *CVPR*, 2022. 2
- [75] Jianwei Yang, Devi Parikh, and Dhruv Batra. Joint unsupervised learning of deep representations and image clusters. In *CVPR*, 2016. 2
- [76] Fisher Yu, Haofeng Chen, Xin Wang, Wenqi Xian, Yingying Chen, Fangchen Liu, Vashisht Madhavan, and Trevor Darrell. Bdd100k: A diverse driving dataset for heterogeneous multitask learning. In *CVPR*, 2020. 4, 12
- [77] Jiahui Yu, Zirui Wang, Vijay Vasudevan, Legg Yeung, Mojtaba Seyedhosseini, and Yonghui Wu. Coca: Contrastive captioners are image-text foundation models. *arXiv preprint arXiv:2205.01917*, 2022. 1
- [78] Lu Yuan, Dongdong Chen, Yi-Ling Chen, Noel Codella, Xiyang Dai, Jianfeng Gao, Houdong Hu, Xuedong Huang, Boxin Li, Chunyuan Li, et al. Florence: A new foundation model for computer vision. *arXiv preprint arXiv:2111.11432*, 2021. 1
- [79] Sukmin Yun, Hankook Lee, Jaehyung Kim, and Jinwoo Shin. Patch-level representation learning for self-supervised vision transformers. In *CVPR*, 2022. 2
- [80] Shuangfei Zhai, Navdeep Jaitly, Jason Ramapuram, Dan Busbridge, Tatiana Likhomanenko, Joseph Yitan Cheng, Walter Talbott, Chen Huang, Hanlin Goh, and Joshua Susskind. Position prediction as an effective pretraining strategy. 2022. 2, 6, 7
- [81] Xiaohua Zhai, Alexander Kolesnikov, Neil Houlsby, and Lucas Beyer. Scaling vision transformers. In *CVPR*, year=2022. 1, 5, 6, 13
- [82] Xiaohua Zhai, Joan Puigcerver, Alexander Kolesnikov, Pierre Ruysen, Carlos Riquelme, Mario Lucic, Josip Djolonga, Andre Susano Pinto, Maxim Neumann, Alexey Dosovitskiy, et al. A large-scale study of representation learning with the visual task adaptation benchmark. *arXiv preprint arXiv:1910.04867*, 2019. 5
- [83] Bolei Zhou, Hang Zhao, Xavier Puig, Sanja Fidler, Adela Barriuso, and Antonio Torralba. Scene parsing through ade20k dataset. In *CVPR*, 2017. 1, 4, 12, 14
- [84] Jinghao Zhou, Chen Wei, Huiyu Wang, Wei Shen, Cihang Xie, Alan Yuille, and Tao Kong. ibot: Image bert pre-training with online tokenizer. *arXiv preprint arXiv:2111.07832*, 2021. 2, 4, 5, 8, 12, 13
- [85] Adrian Ziegler and Yuki M Asano. Self-supervised learning of object parts for semantic segmentation. In *CVPR*, 2022. 1, 2, 3, 8

Table 7. **Comparison with supervised pretrainings** by disentangling localization and classification on semantic segmentation. We report classification only with a frozen backbone (“Classif.”: mAP), localization only (“Loc”: mIoU) and semantic segmentation end-to-end finetunings (“Both”: mIoU) on ADE20k (“A”) and Pascal Context (“P”). Results for ADE20k are also presented in the main paper. LOCA yields excellent locality and good semantic understanding. It is behind supervised image-level pretraining on the pure semantic axis (classification) but better on segmentation (“Both”).

Method	Data	Sup.	Classif.		Loc.		Both	
			A	P	A	P	A	P
<i>ViT-Base/16</i>								
CLIP [53]	WIT	Text	58.3	67.1	66.4	73.2	45.9	52.8
AugReg [60]	Im21k	Labels	60.7	66.1	67.4	75.0	48.1	55.7
LOCA	Im21k	∅	50.2	63.9	68.5	76.5	48.5	55.7
<i>ViT-Large/16</i>								
AugReg [60]	Im21k	Labels	60.3	65.8	68.0	75.4	50.7	56.5
LOCA	Im21k	∅	51.6	63.3	71.0	78.9	52.3	60.3

Appendix

A. Implementation and Evaluation Details

A.1 LOCA pretraining details

We train our models with a base learning rate of 0.001 (linearly ramped up during the first 15 epochs before cosine decay), a batch size of 1024 and a weight decay of 0.1 with adamw optimizer [43]. Models for ablations and analyses are trained during 100 epochs while checkpoints for main results are trained for 600 epochs. 100 epochs of training on 16 TPUv2 accelerators take 29 hours. We use $\eta = 0.8$ for masking. For data augmentation we apply random resized crop, horizontal flipping and color jittering (following the parameters from BYOL [32]). Momentum parameter is set to 0.996 and increased with a cosine schedule to 1 during training [13, 32, 84]. We typically use 10 queries per reference view. We follow MSN pipeline for generating query views [4]. In particular, we restrain the spatial extent of the queries thanks to token dropping. Specifically, one query undergoes random token dropping while the other queries have focal random token dropping. Results are reported with the weights from the momentum branch [13, 84]. We implement LOCA in Jax using the open-sourced SCENIC library [24]. Code and models to reproduce our results will be made publicly available as a SCENIC project.

A.2 Eleven semantic segmentation datasets

In this paper, we report results on the following diverse semantic segmentation benchmarks: ADE20k [83], Pascal Context (“P.Cont”) [48], Pascal VOC (“P.VOC”) [28], Cityscapes (“Citys.”) [20], Berkeley Deep Drive

(“BDD”) [76], CamVid [8], India Driving Dataset (“IDD”) [67], KITTI [1], SUN-RGB-D (“SUN”) [59], IS-PRS [44] and SUIM [38]. We detail the main four datasets used in this paper here and refer to corresponding papers and to Mensink *et al.* [45] for details on the remaining other datasets.

ADE20K [83]. It is a dataset containing scenes with fine-grained labels with 150 semantic classes and is one of the most challenging semantic segmentation datasets. The training split is composed of 20,210 images. We report results on the validation set, composed of 2,000 images.

Pascal Context [48]. The training split is composed of 4,998 images with 59 semantic classes and a background class (hence a total of 60 classes). The validation set has 5,105 images.

Pascal VOC [28]. This dataset has a training set of 10,582 images and counts 21 classes (with background class). We report results on the validation set, it has 1,449 images.

Cityscapes [20]. The dataset contains 5,000 images from 50 different cities. We consider the setup with 19 classes as in [61]. There are 2,975 images in the training set, 500 images in the validation set and 1,525 images in the test set (not used). We report results on the validation set.

A.3 Evaluation protocol

We hope to use a simple decoder for semantic segmentation for better investigating the effectiveness of pretraining. We precisely follow the experimental setup of Segmenter [61] for end-to-end finetuning of Vision Transformer with linear decoder. The data augmentation used during training is normalization, random resizing of the image to a ratio between 0.5 and 2.0, photometric jittering and random horizontal flipping. We randomly crop images and use padding to preserve aspect ratio. We use the 512×512 resolution for all datasets and 768×768 on Cityscapes. On ADE20k, we train for 127 epochs with minibatch size of 16 (resulting in 160k iterations). On Pascal, we train for 256 epochs with minibatch size of 16 (resulting in 80k iterations). On Cityscapes, we train for 215 epochs with minibatch size of 8 (resulting in 80k iterations). On all other datasets, we train with minibatch size of 16 and 160k iterations. We use the “poly” learning rate decay schedule and sweep the base learning rate in $\{8e - 5, 1e - 4, 3e - 4, 8e - 4\}$ for all of our runs. Weight-decay is kept fixed at 0.01. At evaluation time, we use the sliding-window mechanism with window resolution matching the resolution used during training (i.e. 512×512 for all datasets and 768×768 for Cityscapes) to handle varying image sizes during inference. Table 3 row 6 in Segmenter paper [61] reports 48.06 mIoU (single scale) for finetuning from ViT-B/16 AugReg checkpoint [60]. The average of 3 runs in the same setup in our codebase gives

Table 8. **Comparison with previous results on 11 semantic segmentation datasets.** We report mean IoU on the validation set of different semantic segmentation benchmarks. Backbones are pretrained using different self-supervised and supervised methods. We consider two settings: (i) pretraining on ImageNet-1k with ViT-Base/16 and (ii) pretraining on ImageNet-21k with ViT-Large/16. We follow the experimental setup of Segmenter [61] for end-to-end finetuning with linear decoder. We report official numbers from [61] when available and run the evaluation from official released checkpoints when not available. We report the average over 5 runs with single-scale mode (*: with multi-scale evaluation). Finally, we report in the last column the relative improvement over starting from random initialization averaged over the 11 datasets (“avg.rel Δ ”).

Pretraining method	Labels	<i>Consumer</i>			<i>Driving</i>					<i>Indoor</i>	<i>Aerial</i>	<i>Underwater</i>	Avg. rel. Δ (%)
		ADE20k	P.Cont	P.VOC	Citys.	BDD	CamVid	IDD	KITTI	SUN	ISPRS	SUIM	
<i>ImageNet-1k / ViT-Base/16</i>													
Random init.		21.1	19.6	29.1	51.4	40.2	43.3	45.2	39.0	19.7	28.1	53.0	0
DeiT [61, 64]	✓	47.1	–	–	–	–	–	–	–	–	–	–	–
DeiT-III [65]	✓	47.3	53.9	76.1	79.7	62.7	53.8	55.4	47.2	47.5	42.1	73.5	+79.0
DINO [13]		44.1	50.7	74.1	78.4	60.7	51.5	54.3	46.4	44.4	41.5	71.2	+71.9
MoCo-v3 [17]		45.4	51.6	74.5	78.6	60.4	51.1	53.7	45.7	45.6	42.1	72.6	+73.6
iBOT [84]		47.0	54.6	75.0	79.8	62.1	51.5	55.5	47.0	46.3	42.2	73.2	+77.7
MAE [34]		45.5	51.7	75.0	79.7	62.1	57.8	55.8	48.3	45.9	44.6	72.4	+77.8
LOCA (Ours)		47.9	54.9	76.7	79.8	62.8	56.1	55.6	48.5	47.7	45.6	74.0	+82.1
<i>ImageNet-21k / ViT-Large/16</i>													
Random init.		21.2	20.1	31.1	44.9	39.7	43.7	45.4	39.7	19.2	26.7	48.3	0
Augreg [60, 61]	✓	50.7	56.5*	77.5	80.7*	62.3	51.2	54.9	47.6	48.5	43.8	73.7	+84.8
LOCA (Ours)		52.3	60.3	78.7	81.5	65.3	56.0	57.5	50.3	51.3	49.7	73.7	+93.9

48.07 mIoU (run 1: 48.41, run 2: 48.08, run 3: 47.70). This validates our reproduction of the linear decoder presented in the Segmenter work [61].

B. Additional Results

B.1 Comparison on 11 semantic segmentation tasks

In Table 8, we compare LOCA pre-training to different self-supervised and supervised methods on eleven semantic segmentation benchmarks with diverse properties and domains. The datasets and evaluation protocols are detailed in Sections A.2 and A.3. With ViT-Base/16 architecture and ImageNet-1k dataset, the relative improvement over starting from random initialization averaged over the 11 datasets for LOCA features is +82.1%. This is +4.8 points above the best self-supervised competitor, MAE, and +3.1 points above supervised pretraining with DeiT-3. With ViT-Large/16, LOCA features transfer even better to semantic segmentation. They reach a relative improvement over random initialization of +93.9%, which is 9.1 points higher than the results obtained with AugReg checkpoint [60] in the Segmenter paper [61]. This validates our location-aware pretraining for transferring on semantic segmentation downstream tasks compared to using checkpoints pretrained with a supervised, global task such as AugReg [60].

B.2 More localization/classification trade-off results

Semantic segmentation is the coupling of classification and localization, where these two tasks can have different feature preferences. In this section, we propose to disentangle classification and localization performance on semantic segmentation benchmarks which require both. First, we discard local information and evaluate classification only by training a linear layer with a multi-label binary cross-entropy loss. Second, we evaluate localization only by reporting the performance of an already finetuned semantic segmentation model in presence of a class oracle. Specifically, the oracle replaces the label of each mask by the label of the ground truth mask it has the best IoU with. This evaluation allows to assess the shape and localization of the predictions but not their class.

Comparison with image-level supervised pretrainings.

We compare our self-supervised location-aware pretraining to two powerful image-level pretraining paradigms: (i) image classification (i.e. label supervision) as in [60, 81] and (ii) image-text alignment as in CLIP [53]. We present the results by disentangling localization and classification on semantic segmentation. Note that we report classification with a frozen backbone as typically done in self-supervised learning literature (coined as the “linear probing” evaluation protocol). In Table 3 of the main paper, we have reported results only with ADE20k dataset. We show in Table 7 that observations and conclusions are consistent when consider-

Table 9. **Disentangling localization and classification on semantic segmentation.** We report end-to-end finetuning on classification only (with a multi-label classification loss) and localization only (with an oracle giving the class of the segmentation masks) evaluations on 4 popular semantic segmentation benchmarks: ADE20k [83], Pascal Context (“P.Cont.”) [48], Pascal VOC (“P.VOC”) [28] and Cityscapes (“City.”) [20]. Best number is in bold and second best is underlined. We report performance for different methods pretrained on ImageNet-1k (with or without labels) with ViT-B/16.

Method	Classification only (mAP)				Localization only (mIoU)				Both (mIoU)			
	ADE20k	P. Cont.	P. VOC	Citysc.	ADE20k	P. Cont.	P. VOC	Citysc.	ADE20k	P. Cont.	P. VOC	Citysc.
<i>Image-level pretrainings</i>												
DINO [13]	61.6	67.7	89.9	81.5	64.5	71.6	78.7	79.6	44.1	50.7	74.1	78.4
MoCo-v3 [17]	61.1	69.3	93.6	82.1	66.2	73.7	79.0	79.9	45.4	51.6	74.5	78.6
Supervised (DeiT-III [65])	64.8	71.5	94.6	<u>84.0</u>	66.5	73.6	<u>80.1</u>	80.7	<u>47.3</u>	<u>53.9</u>	<u>76.1</u>	<u>79.7</u>
<i>Spatially-aware pretrainings</i>												
MAE [34]	59.0	67.6	92.8	84.3	<u>67.0</u>	<u>74.3</u>	79.9	<u>81.1</u>	45.5	51.7	75.0	<u>79.7</u>
LOCA (Ours)	<u>62.2</u>	<u>69.9</u>	<u>93.7</u>	83.6	67.9	75.4	80.5	81.4	47.9	54.9	76.7	79.8

ing other datasets, namely Pascal Context and Cityscapes. On Pascal Context, we interestingly observe in Table 7 that the final performance on semantic segmentation is the same for AugReg and LOCA ViT-B/16 checkpoints pretrained on ImageNet-21k (i.e. 55.7 mIoU). However, this performance can be explained by different factors for the two checkpoints: (i) good classification performance for AugReg (i.e. 66.1 for AugReg vs 63.9 for LOCA) and (ii) acute localization performance for LOCA (i.e. 75.0 for AugReg vs 76.5 for LOCA).

Comparison with different supervised and self-supervised pretrainings. In Table 9, we compare the behavior of models pretrained with an image-level versus spatially-aware objective with ViT-B/16 on ImageNet-1k. Unlike previous experiment in Table 7, we report end-to-end finetuning for classification only in this experiment. Indeed, we have observed that freezing the backbone and training a linear classifier on top of MAE features perform very poorly [34]. In Table 9, we observe that models pretrained with a global, image-level objective such as DeiT-III or MoCo-v3 tend to be better on the classification aspect. By contrast, models trained with a spatially-aware objective such as MAE or LOCA produce more spatially accurate predictions. Overall, LOCA yields excellent locality and good class-level understanding (while not beating representations learned with label classification pretraining [65] on the pure classification axis). This results in strong semantic segmentations which require both locality and semantic features.

B.3 Scaling Study

We report in Table 10 (resp. in Table 11) the numbers corresponding to Figure 2 (left) (resp. (right)) of the main paper. We observe that the performance boost from increasing the

Table 10. **Scaling in data axis** on ImageNet-21k. We report performance (mean IoU on ADE20k - single scale evaluation) for different pretrained LOCA models. “Rand- x ” means that we take a random subset of size x in ImageNet-21k. “INet-1k” means that we use the ImageNet-1k dataset only for pretraining.

Arch / Data	Rand-130k	Rand-1.3M	Full 13M	INet-1k
ViT-Base/16	41.4	46.9	48.5	47.9
ViT-Large/16	39.1	48.5	52.3	49.6

Table 11. **Scaling in model axis** on ImageNet-21 and ImageNet-1k. We report performance (mean IoU on ADE20k - single scale evaluation) for different pretrained LOCA models. The performance boost from increasing the pretraining dataset size increases when considering bigger architectures.

Data / Arch	Small/16	Base/16	Large/16	Huge/16
ImageNet-1k	44.8	48.0	49.6	48.9
ImageNet-21k	44.8 (+0.0)	48.5 (+0.5)	52.3 (+2.7)	54.3 (+5.4)

pretraining dataset size increases when considering bigger architectures.

C. Visualizations

In this section, we visualize the output of the position prediction pretraining task. Specifically, in Figure 7, we visualize query location prediction for different LOCA models. We compare models pretrained with different masking rates: (i) $\eta = 0$: no masking, the reference is entirely visible to the query; (ii) $\eta = 0.8$: default masking rate, only 40 reference patch tokens are visible to the query; (iii) $\eta = 1$: full masking, the reference is invisible to the query.

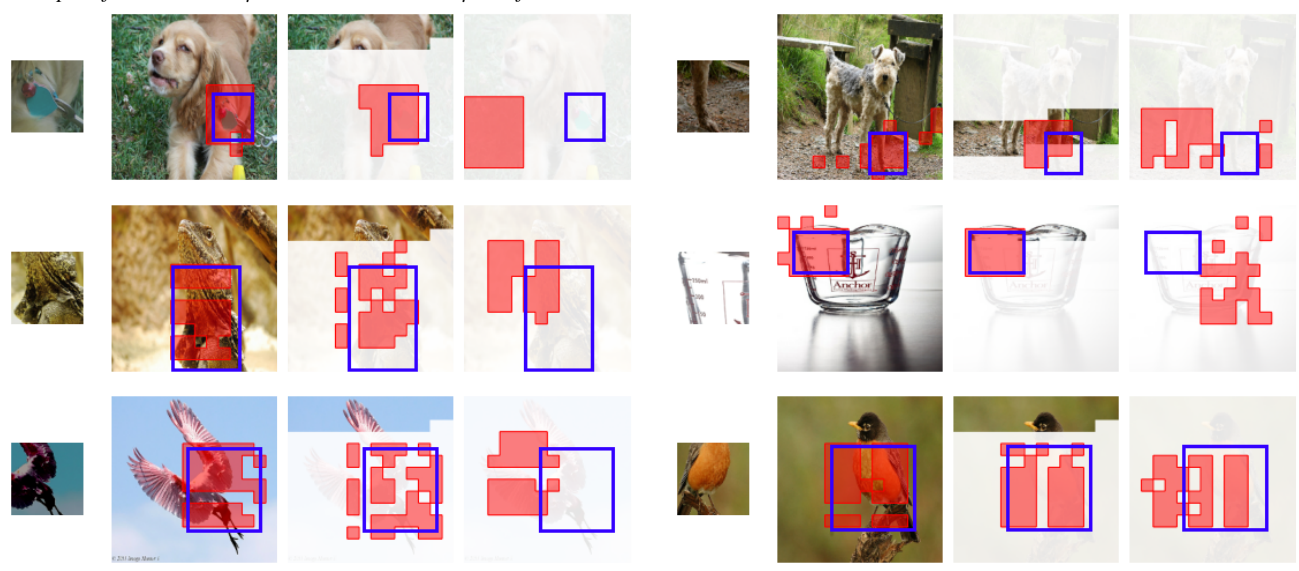
In the first rows of Figure 7, we show examples where the network seems to effectively solve the task by *relative location*. In those cases, we observe that LOCA trained with

masking rate $\eta = 0.8$ manages to locate the query based on the patches visible from the reference. For example we see that the network successfully manages to locate the leash joint based on seeing the patch representations of the head of the dog, or to locate the neck of the lizard based on the visible patches of its head. By contrast, the network which does not see the reference at all (i.e. $\eta = 1$) cannot successfully locate the query in those cases. Interestingly, we see that in some cases, this network ($\eta = 1$) can still locate the query by learning where things are typically located in natural images. For example, we observe in Figure 7 that by recognizing a part such as “ear” it makes a guess that it is more likely to be at the top of the image rather than at the bottom. However, it cannot guess if it is left or right because we apply random horizontal flips between query and reference during training and so this patch is as likely to occur at the right than at the left of the image.

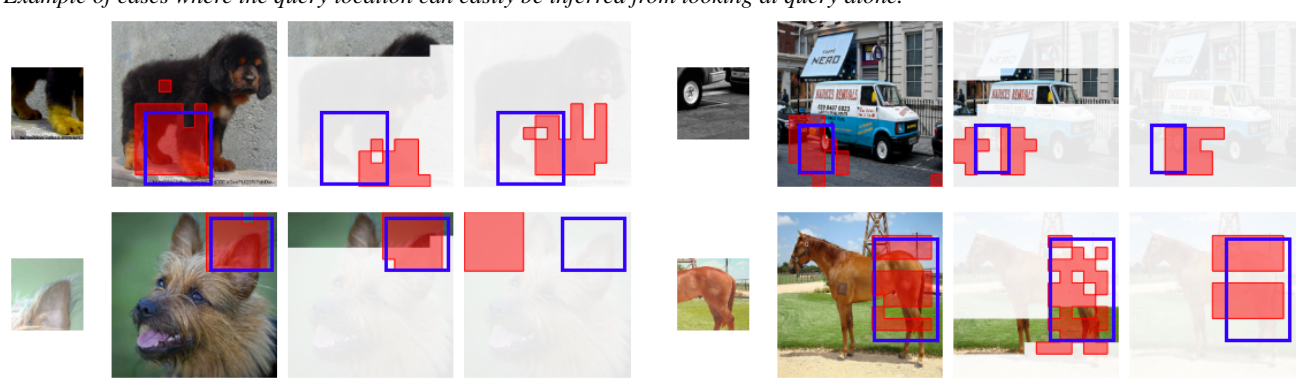
Lastly, we observe that the network trained with full access to the reference ($\eta = 0$) can almost always locate the query. This is because it can rely on low-level cues such as edge consistency or salient points. The last rows of Figure 7 illustrate this phenomenon.

query $\eta = 0$ $\eta = 0.8$ $\eta = 1$ query $\eta = 0$ $\eta = 0.8$ $\eta = 1$

Example of cases where $\eta = 0.8$ succeeds and $\eta = 1$ fails. The network relies on relative location.



Example of cases where the query location can easily be inferred from looking at query alone.



Example of cases where the network relies on low-level cues. Only the variant with $\eta = 0$ succeeds.

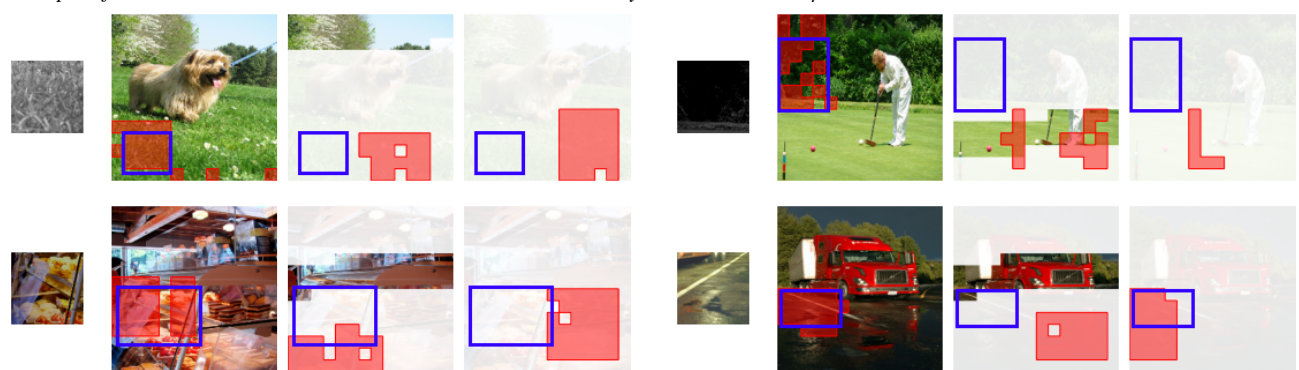


Figure 7. **Visualizing LOCA’s position predictions.** The query location is shown in blue in the reference and LOCA predictions are shown in red. Columns correspond to different reference masking rates and we show only patches visible to the query when it makes its prediction. Displayed images are not seen during training. See discussion in Section C.